

Arginine-assisted Thermal Decomposition for Synthesis of Nanosized Co_3O_4 with Enhanced Capacitance

Ruyi Zou^{1,2}, Lin Zhu¹, Guiling Luo¹, Yanyan Niu¹, Hui Xie¹, Ruixia Dong¹, Hui Cheng¹, Wei Sun^{1,*}, Laijun Zhang²

¹ Key Laboratory of Laser Technology and Optoelectronic Functional Materials of Hainan Province, Key Laboratory of Functional Materials and Photoelectrochemistry of Haikou, College of Chemistry and Chemical Engineering, Hainan Normal University, Haikou 571158, P R China

² Jiangxi Province Key Laboratory of Polymer Preparation and Processing, School of Chemistry and Environmental Sciences, Shangrao Normal University, Shangrao 334001, China

*E-mail: sunwei@hainnu.edu.cn

Received: 7 September 2019 / Accepted: 2 November 2019 / Published: 30 November 2019

Arginine-assisted thermal decomposition technique was used to prepare nanosized Co_3O_4 (A- Co_3O_4) with its supercapacitive performances checked. A- Co_3O_4 was characterized by different techniques such as X-ray diffraction, X-ray photoelectron spectroscopy, Fourier transform infrared spectroscopy and scanning electron microscopy. Brunauer-Emmett-Teller analysis revealed that A- Co_3O_4 had a larger specific surface area than Co_3O_4 prepared by conventional calcination without arginine (F- Co_3O_4). Electrochemical performances of A- Co_3O_4 based electrode were better than that of the F- Co_3O_4 based electrode. Cyclic voltammetric results showed the specific capacitances of A- Co_3O_4 and F- Co_3O_4 were found to be 259.2 and 122.2 F/g at a scan rate of 0.01 V/s. Long-term galvanostatic charge-discharge cycling tests indicated the specific capacitance for A- Co_3O_4 and F- Co_3O_4 were 128.6 F/g and 106.4 F/g with 104.7% and 103.3% capacitance retention after 1000 cycles at a current density of 5.0 A/g. Electrochemical impedance spectra analysis showed the charge transfer resistance (R_{ct}) of A- Co_3O_4 was 7.56 Ω and that of F- Co_3O_4 was 15.56 Ω . All the results indicated the A- Co_3O_4 exhibited superiority originated from large surface area with porous structure.

Keywords: Supercapacitor; Electrochemistry; Nanosized Co_3O_4 ; Thermal decomposition; Arginine

1. INTRODUCTION

Supercapacitors have been the research focuses because of its higher power density, longer cycle lifetime and less maintenance cost compared with secondary batteries [1,2], which can be applied in many fields such as distributed energy sources devices for communication and military. Though the performance of core capacitor materials determines the quality of supercapacitors [3],

researchers have tried substances of various components and novel preparation methods to meet the requirements of supercapacitors. It is well-known that Co_3O_4 with spinel configuration has high theoretical specific capacitance (3650 F/g) and is an excellent candidate material [4]. However, the small specific surface area or semi-conductivity of Co_3O_4 limits the full display of its theoretical capacitance, which becomes one of the obstacles to its wide utilization [5]. Various approaches and strategies have been devised for increasing the specific capacitance of the electrode materials, including unique morphology, mesoporous features, and 3D hierarchical structures. The specific morphology of Co_3O_4 can greatly improve its performance as electrode materials for supercapacitor with their electrochemical properties evaluated. For example, 3D hierarchical flower-like Co_3O_4 assembled by hexagonal nanosheets exhibited higher specific capacitance (327.3 F/g at 0.5 A/g) with excellent retention (96.07% at 5 A/g) after 10000 cycles [6]. Yuan et al. proved that the improved supercapacitor performances were due to its unique hierarchically porous morphological characteristics by using hierarchically porous Co_3O_4 film with a thickness of 15-20 nm and multiple mesoporous walls ranging from 2 to 3 nm, which exhibited superior supercapacitive performances with high specific capacitances (443 F/g at 2 A/g and 334 F/g at 40 A/g) [7]. Yin et al. reported $\text{Co}(\text{OH})_2/3\text{D}$ graphene nanocomposite with a superior specific capacitance of 730.23 mF/cm² at the current density of 5 mA/cm², and 79.83% of the specific capacitance was retained after 3000 cycles at the current density of 20 mA/cm² [8]. Despite those research efforts, the development of simple, cost-effective, greenly methods for preparation Co_3O_4 materials with suitable morphology, size, porosity and good performance is still challenging [9].

In general, various methods including ball milling [10], high shear mixing [11] or ultrasonication [12,13] have been used to break up agglomerated nanoparticles [14] with the further enhancement of the electrochemical property mainly through increasing specific surface area. In this work, arginine assisted thermal decomposition process was used to prevent agglomeration of Co_3O_4 materials. By mixing arginine with the precursor and heating together, arginine could generate gas during thermal decomposition, thereby making the nanomaterial loose and enriching the pores in the bulk phase with the increase of specific surface area. The procedure was different from the conventional morphology control-synthesis. With enlarged surface area the physical properties of two kinds of Co_3O_4 prepared by thermal decomposition with or without arginine-assisted were compared, and the capacitance property of nanosized Co_3O_4 was discussed in detail.

2. EXPERIMENTAL

2.1. Reagent

L-arginine (Shanghai Aladdin Ltd. Co., China), cobalt (II) chloride hexahydrate (Shantou Xilong Chemical Factory, China) and malonic acid (Sinopharm. Chem. Reagent Ltd. Co., China) were used as received. Other chemicals were of analytical grade and doubly distilled water was used to prepare all the solutions.

2.2. Materials synthesis

50 mL 0.2 mol/L sodium carbonate solution was mixed with 50 mL 0.2 mol/L cobalt chloride solution to form purple flocculent precipitate, which was centrifuged and washed with water for several times. The precipitate was dissolved in 50 mL of 0.2 mol/L malonic acid solution, which gave a large number of bubbles from the liquid with a purple-red solution formed. Then this solution was placed in a 90 °C water bath to slowly evaporate the solvent. Finally, the obtained solid was dried at 60 °C, mixed with arginine at a mass ratio of 1:1, and thoroughly grounded in an agate mortar. Lastly, this mixture was calcined at 400 °C for 3 hours in a muffle furnace to obtain nanosized Co_3O_4 , which was designated as A- Co_3O_4 . The control sample (designated as F- Co_3O_4) was prepared in the same manner except that the thermal decomposition process was not assisted by the addition of arginine.

2.3. Structural characterization

The microstructures and morphologies of nanosized Co_3O_4 were studied on a scanning electron microscopy (SEM, JSM-7100F, JEOL, Japan) and field emission transmission electron microscopy (HRTEM, JEM-2100F, JEOL, Japan). X-ray photoelectron spectroscopy (XPS, Escalab 250XI, Thermo Fisher Scientific Inc., USA) was used to determine the element type and composition content of samples. The crystal structure was evaluated on a powder X-ray diffraction (XRD) system (Miniflex II, Rigaku, Japan) with $\text{Cu K}\alpha$ radiation. Fourier transform-infrared (FT-IR) spectrum was measured on a Nicolet 6700 FT-IR spectrophotometer (Thermo Fisher Scientific Inc., USA). Nitrogen absorption/desorption isotherms were obtained on a Autosorb-iQ-C analyzer (Quantachrome Instruments, USA) at 77.35K and the corresponding surface areas were determined using the Brunauer–Emmett–Teller (BET) method, and pore size distribution was estimated using the Barrett–Joyner–Halenda (BJH) method.

2.4. Electrode preparation and electrochemical measurements

A Metrohm Autolab (PGSTAT 302N, Metrohm, Netherlands) electrochemical workstation was employed to evaluate electrochemical properties with different methods including cyclic voltammetry (CV), galvanostatic charge-discharge (GCD), long-term cycling tests and electrochemical impedance spectroscopy (EIS), respectively. CV measurements were carried out in the scan range from -0.2 to 0.8 V (vs. Hg/HgO) at scan rate of 0.01, 0.04, 0.07 and 0.10 V/s. GCD tests were performed in the voltage range of -0.4~0.6 V (vs. Hg/HgO) at different current densities range of 2.5, 5.0, 7.5, 10.0, 12.5 and 15.0 A/g. EIS measurements were carried out in the frequency range of 0.01 Hz to 100 kHz at the open circuit potentials, and the applied potential amplitude was 5 mV. All of these tests were conducted using a three-electrode system with 6.0 mol/L KOH as electrolyte. The freshly prepared Co_3O_4 modified electrode, a platinum wire electrode, and a Hg/HgO electrode were used as the working electrode, counter electrode, and reference electrode, respectively.

The working electrode was prepared by using the mixture of as-prepared Co_3O_4 (80 wt%), acetylene black (10 wt%) and polyvinylidene fluoride (PVDF, 10 wt%), which was first coated onto

the surface of nickel foam sheet (1.0 cm × 1.0 cm), and then dried at 80 °C for 12 h. The nickel foam sheets with active materials were pressed under 8 MPa to obtain the working electrode. The loading mass of active material was around 2.5 mg/cm².

The specific capacitance is calculated from the following equation:

$$C = \frac{\int_{V_1}^{V_2} i dV}{v \times m \times \Delta V} \quad (1)$$

$$C = \frac{i \times \Delta t}{\Delta V \times m} \quad (2)$$

Where C (F/g) is the specific capacitance, *i* (A) is the discharge current, Δt (s) is the discharge time, ΔV (V) represents the potential windows, *v* (V/s) is the scan rate, and *m* (g) is the mass of the active material.

After the data were obtained from CV measurements, specific capacitance values could be calculated by equation (1). And if data was from GCD measurements, equation (2) could be used.

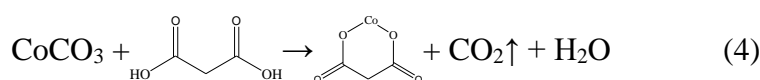
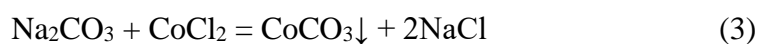
3. RESULTS AND DISCUSSION

3.1 Characterizations

Figure 1 (A-C) showed the SEM images of precursors, F-Co₃O₄ and A-Co₃O₄, respectively. The precursor was present as a quadrangular prism (Figure 1 A). After calcination at 400°C, the precursor decomposed into an ellipsoidal product made up of many Co₃O₄ nanoparticles (Figure 1 B). If the thermal decomposition was assisted with arginine, the ellipsoidal structure would be broken with many holes present (Figure 1C). Figure 1D was the HRTEM image of A-Co₃O₄, from which it could be estimated that the particle size of A-Co₃O₄ was between 30 and 80 nm. And parallel stripes with a pitch of 0.46 nm were shown in Figure 1E, corresponding to the (111) crystal plane of spinel Co₃O₄ [15].

XPS survey spectrum of A-Co₃O₄ (a) and F-Co₃O₄ (b) in Figure 1F showed that the elemental compositions of two as-prepared Co₃O₄ were identical, which identified the main elements of Co and O with the impurity elements such as C, Na and Cl. The crystal structure and phase of F-Co₃O₄ and A-Co₃O were identified by XRD. As shown in Figure 1G, XRD patterns of F-Co₃O₄ and A-Co₃O were consistent, confirming to be the same substance with crystal structure and phase in accordance with cubic cobalt oxide (PDF#71-0816). Therefore, the results of XPS and XRD both proved that the samples were oxides of cobalt.

Figure 1H was the X-ray diffraction spectrum of the precursor and peaks were indexed using the JCPDS data card (PDF#26-1647), confirming the cobalt malonate was the main component of the precursor. Therefore, it was possible for the formation of the precursor according to the following equations:



The reaction of CO_3^{2-} with Co(II) resulted in the formation of precipitate (CoCO_3 , as shown in equation 3), which was further reacted with malonic acid to get the cobalt malonate with CO_2 released (equation 4).

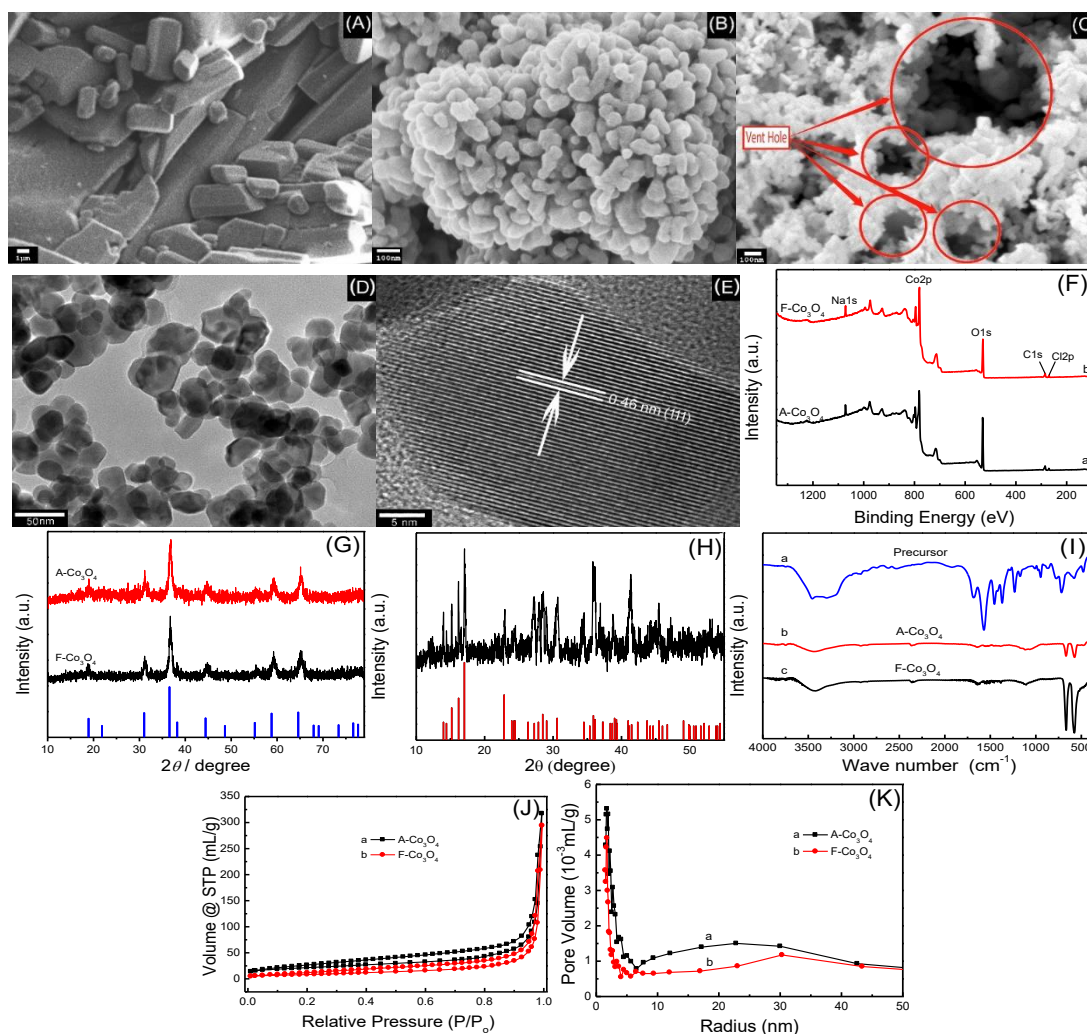


Figure 1. SEM images of (A)precursor, (B) F- Co_3O_4 and (C) A- Co_3O_4 ; TEM images of (D and E) A- Co_3O_4 ; (F)XPS survey spectrum of A- Co_3O_4 (a) and F- Co_3O_4 (b); XRD patterns of (G) A- Co_3O_4 , F- Co_3O_4 and (H) precursors; (I) FT-IR for precursor (a), A- Co_3O_4 (b) and F- Co_3O_4 (c); (J) N_2 adsorption/desorption isotherm and (K) pore size distribution of A- Co_3O_4 and F- Co_3O_4 .

Figure 1 I showed the infrared spectra of precursor (a), A- Co_3O_4 (b) and F- Co_3O_4 (c), respectively. The peaks at 1568 cm^{-1} and 1385 cm^{-1} of curve (a) were asymmetric stretching and symmetric stretching peaks of carboxylate ions (COO^-), which meant that cobalt carboxylate was formed. Curve (b) was similar to curve (c), indicating that A- Co_3O_4 and F- Co_3O_4 were the same substance. The result were supported by the XPS and XRD analysis, and infrared peaks at 560 cm^{-1} and 660 cm^{-1} were corresponded to $\text{Co}^{2+}\text{-O}$ and $\text{Co}^{3+}\text{-O}$, respectively.

Because the large specific surface can increase the contact area between the material and the electrolyte, the specific surface area of the active electrode nanomaterials have great influence on the capacitance [16,17]. The BET and BJH method were utilized to calculate the specific surface area and

the pore volume distribution of A-Co₃O₄ and F-Co₃O₄ nanoparticles [18], respectively. As shown in Figure 1J and K, the N₂ sorption isotherms of A-Co₃O₄ and F-Co₃O₄ were classified as type IV with a sharp H3 hysteresis loop, suggesting the presence of mesopores with the specific surface area of 76.4 m²/g and 32.3 m²/g, respectively, and the most probable pore radius were about 1.75 nm for both of them. A-Co₃O₄ had a larger specific surface area than F-Co₃O₄ because arginine was converted into a large amount of gas during thermal decomposition, and these gases were expanded to break up Co₃O₄ aggregates, as marked area in Figure 1C with the vent hole.

3.2 Electrochemical properties

Electrochemical performances of A-Co₃O₄ and F-Co₃O₄ were evaluated by various electrochemical techniques. Figure 2A presented the CV curves of A-Co₃O₄ electrode (a) and F-Co₃O₄ electrode (b) at the scan rate of 0.01 V/s. Both of them had two pair of reversible redox peaks, which were corresponded to the conversions between different cobalt oxidation states with the following equation (5) and equation (6) [19].



Figure 2 A also showed that the enclosed area of curve a was larger than that of curve b, which revealed that the larger specific capacitance of A-Co₃O₄ electrode than F-Co₃O₄ electrode. And the specific capacitances of A-Co₃O₄ and F-Co₃O₄ electrode were found to be 259.2 F/g and 122.2 F/g. Figure 2 B and C showed the CV curves of A-Co₃O₄ electrode and F-Co₃O₄ electrode at different scan rates. It can be seen that the increase of scan rate lead to the increase of the redox peak currents, which implied that the electrochemical capacitances of these two Co₃O₄ materials were resulted from a typical Faradaic processes with good redox reversibility of fast charge/discharge response [20].

Table 1. Comparison of specific capacitance of various morphologies Co₃O₄ based electrodes.

Morphology	Method	Electrolyte	Specific capacitance	Potential window	Scan rate	Reference
crater-like	template	1 M KOH	102.0 F·g ⁻¹	0.1~0.6 V (vs. Hg/HgO)	3 mV·s ⁻¹	[22]
flower-like	solvothelmal	6 M KOH	131.7 F·g ⁻¹	-0.2~0.4 V (vs. Hg/HgO)	1 mV·s ⁻¹	[23]
nanowire	hydrothelmal	2 M KOH	251 F·g ⁻¹	0.1~0.6 V (vs. SCE)	1 mV·s ⁻¹	[24]
nanorods	hydrothelmal	6 M KOH	226.3 F·g ⁻¹	-0.4~1.0 V (vs. Ag/AgCl)	10 mV·s ⁻¹	[25]
nanoparticle	precipitation	6 M KOH	259.2 F·g ⁻¹	-0.2~0.8 V (vs. Hg/HgO)	10 mV·s ⁻¹	This work

Figure 2 D showed the specific capacitance of A-Co₃O₄ were 259.2, 227.7, 196.4 and 174.2 F/g and those of F-Co₃O₄ were 122.2, 117.4, 112.7 and 108.9 F/g at the corresponding scan rates. And the decrease in their specific capacitances with scan rate increasing, which was attributed to the fact that the electrolyte ions were unable to fully access the interior surfaces of the active materials for charge-storage due to the reduced diffusion time at a high scan rate [21]. The specific capacitance of A-Co₃O₄

electrode was compared with other reported different morphology Co_3O_4 based electrodes with the data shown in table 1. It was worthwhile to note that the better pseudo-capacitance performance of A- Co_3O_4 electrode was attributed to the large specific surface A- Co_3O_4 obtained from the proposed synthesis procedure.

GCD curves of A- Co_3O_4 electrode and F- Co_3O_4 electrode at different current densities ranging from 2.5 to 15.0 A/g were shown in Figure 2E and F, which could estimate the capacitance of the Co_3O_4 electrodes. These approximately mirrored potential-time specific capacitances implied that the charge/discharge process of these Co_3O_4 electrodes were reversible. The specific capacitances were calculated from GCD curves using equation 2 and shown in Figure 2G, which also proved the higher specific capacitances of A- Co_3O_4 than that of F- Co_3O_4

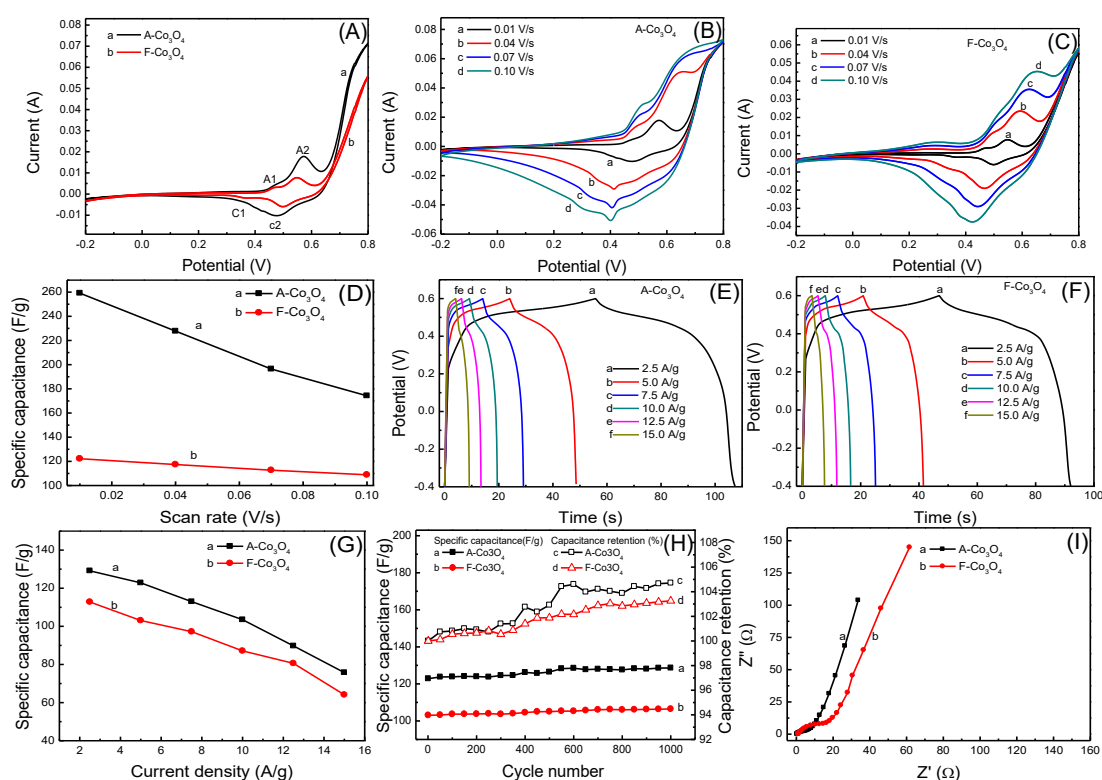


Figure 2. (A) CV curves of A- Co_3O_4 (a) and F- Co_3O_4 (b) electrode at scan rate of 0.01 V/s; CV curves of (B) A- Co_3O_4 and (C) F- Co_3O_4 electrode at different scan rates (a→d: 0.01, 0.04, 0.07, 0.10 V/s); (D) Specific capacitance at different scan rates of A- Co_3O_4 (a) and F- Co_3O_4 ; GCD curves of (E) A- Co_3O_4 and (F) F- Co_3O_4 electrode at different current densities (a→e: 2.5, 5.0, 7.5, 10.0, 12.5 and 15.0 A/g); (G) The discharge specific capacitance of A- Co_3O_4 (a) and F- Co_3O_4 (b) electrode at various current densities (a→e: 2.5, 5.0, 7.5, 10.0, 12.5 and 15.0 A/g); (H) Specific capacitances and capacitance retentions variation of A- Co_3O_4 (a) and F- Co_3O_4 (b) electrode within 1000 GCD cycles at the current density of 5.0 A/g; (I) Nyquist plots of A- Co_3O_4 (a) and F- Co_3O_4 (b) electrode in 6.0 mol/L KOH electrolyte.

The long-term galvanostatic cycling stability was important for supercapacitor electrode materials, which was investigated in a 6.0 mol/L KOH solution at a current density of 5.0 A/g. The variations of capacitance retention rate with cycle number were recorded at intervals of 50 cycles for

1000 cycles with the results shown in Figure 2H. The results showed that their specific capacitances were increase with increasing number of cycles, and the specific capacitances for A-Co₃O₄ and F-Co₃O₄ reached 128.6 F/g and 106.4 F/g with 104.7% and 103.3% capacitance retention after 1000 cycles. A gradual capacitance retention increasement was due to electrochemical activation phenomenon [17,22], which revealed that both Co₃O₄ electrodes had good cycling stability.

The Nyquist plots were obtained by EIS measurements with curves presented in Figure 2 I, which were composed of a semicircle in the high frequency region and a straight line in the low frequency region. The semicircle is related to Faradic reactions attributed to the charge transfer resistance at the electrode/electrolyte interface [23] and the straight line is corresponded to a Warburg impedance related to the diffusion of electrolyte within the pores of the electrode [24]. In Figure 2 I, the charge transfer resistance (R_{ct}) for A-Co₃O₄ was 7.56 Ω , which was lower than that for F-Co₃O₄ (15.56 Ω). At low frequencies, the straight line (Warburg impedance) of A-Co₃O₄ was more perpendicular to the real axis than that of F-Co₃O₄, indicating the lower Warburg resistance for A-Co₃O₄. Therefore, the higher specific surface area of A-Co₃O₄ could facilitate the diffusion of electrolyte ions into the electrode material, resulting in an easy and reversible Faraday redox process.

4. CONCLUSION

Nanosized A-Co₃O₄ was synthesized by thermal decomposition assisted with arginine, which showed better electrochemical properties than that of F-Co₃O₄ synthesized without adjuvant for thermal decomposition. Due to the assist of arginine during thermal decomposition, A-Co₃O₄ had a larger specific surface area than F-Co₃O₄, and as a result, the lower R_{ct} of A-Co₃O₄ electrode and greater specific capacitance at the same current density could be achieved. According to the GCD test results, the specific capacitance of A-Co₃O₄ was 128.6/g and that of F-Co₃O₄ was 106.4 F/g at the current densities of 5 A/g. This work demonstrated that arginine-assisted thermal decomposition was a simple method for disintegrating the agglomeration of nanomaterials.

ACKNOWLEDGEMENTS

This work was financially supported by Graduate Student Innovation Research Project of Hainan Normal University (Hsyx2017-11), National Natural Science Foundation of China (21561028), Foundation of Jiangxi Province Key Laboratory of Polymer Preparation and Processing of Shangrao Normal University (jxsr201602).

References

1. M. Gopalakrishnan, G. Sriresh, A. Mohan, V. Arivazhagan, *Applied Surface Science*, 403 (2017) 578.
2. C. Yuan, J. Li, L. Hou, X. Zhang, W. D. L. Xiong, *Advanced Functional Materials*, 22 (2012) 4592.
3. S. Chen, W. Xing, J. Duan, X. Hu, S. Z. Qiao, *Journal of Materials Chemistry A*,1 (2013) 2941.

4. J. Zhu, B. Huang, C. Zhao, H. Xu, S. Wang, Y. Chen, L. Xie, L. Chen, *Electrochimica Acta*, 313 (2019) 194.
5. X. Liu, S. Shi, Q. Xiong, L. Li, Y. Zhang, H. Tang, C. Gu, X. Wang, J. Tu, *ACS Applied Materials & Interfaces*, 5 (2013) 8790.
6. K. Ding, X. Zhang, P. Yang, X. Cheng, *Crystengcomm*, 18 (2016) 8253.
7. Y. F. Yuan, X. H. Xia, J. B. Wu, X. H. Huang, Y. B. Pei, J. L. Yang, S. Y. Guo, *Electrochemistry Communications*, 13 (2011) 1123.
8. C. X. Yin, W. C. Wan, H. Xie, W. J. Weng, G. J. Li, B. H. Li, Y. B. Wang, X. Q. Wu, W. Sun, *International Journal of Electrochemical Science*, 14 (2019) 4185.
9. H. Jiang, J. Ma, C. Li, *Chemical Communications*, 48 (2012) 4465.
10. S. Yoon, *International Journal of Applied Engineering Research*, 12 (2017) 11765.
11. L. Wang, Y. Cui, B. Li, S. Yang, R. Li, Z. Liu, R. Vajtai, W. Fei, *RSC Advances*, 5 (2015) 51193.
12. M. Zhen, C. Yan, X. Zuo, X. Xin, Y. Sun, R. Zeng, J. Nan, *Electrochimica Acta*, 174 (2015) 1268.
13. H. Li, Q. Chen, J. Zhao, K. Urmila, *Scientific Reports*, 5 (2015) 11033.
14. N. Mandzy, E. Grulke, T. Druffel, *Powder Technology*, 160 (2005) 121.
15. L. H. Hu, Q. Peng, Y. D. Li, *Journal of America Chemistry Society*, 130 (2008) 16136.
16. W. Du, R. Liu, Y. Jiang, Q. Lu, Y. Fan, F. Gao, *Journal of Power Sources*, 227 (2013) 101.
17. L. Jie, X. Li, Y. Luo, Q. Cen, Q. Ye, X. Xu, W. Fan, *International Journal of Hydrogen Energy*, 43 (2018) 9635.
18. T. Zhou, W. Gao, Q. Wang, A. Umar, *Journal of Nanoscience & Nanotechnology*, 18 (2018) 3499.
19. S. A. Pawar, D. S. Patil, J. C. Shin, *Journal of Industrial & Engineering Chemistry*, 54 (2017) 162.
20. J. Xu, L. Gao, J. Cao, W. Wang, Z. Chen, *Electrochimica Acta*, 56 (2010) 732.
21. X. Xing, Y. Gui, G. Zhang, C. Song, *Electrochimica Acta*, 157 (2015) 15.
22. W. Lu, X. Liu, W. Xin, X. Yang, L. Lu, *Current Applied Physics*, 10 (2010) 1422.
23. J. Jiang, W. Shi, S. Song, Q. Hao, W. Fan, X. Xia, Z. Xian, W. Qian, C. Liu, Y. Dan, *J. Power Sources*, 248 (2014) 1281.
24. B. Wang, T. Zhu, H. B. Wu, R. Xu, J. S. Chen, X. W. Lou, *Nanoscale*, 4 (2012) 2145.
25. G. U. Jang, S. Ameen, M. S. Akhtar, E. Kim, H. H. Shin, *Chemistryselect*, 2 (2017) 8941.
26. X. Y. Liu, Y. Q. Zhang, X. H. Xia, S. J. Shi, Y. Lu, X. L. Wang, C. D. Gu, J. P. Tu, *Journal of Power Sources A*, 239 (2013) 157.
27. L. Cui, J. Li, X. G. Zhang, *Journal of Applied Electrochemistry*, 39 (2009) 1871.
28. Y. Gao, S. Chen, D. Cao, G. Wang, J. Yin, *Journal of Power Sources*, 195 (2010) 1757.